Miner Petrol (2017) 111:383–397
DOI 10.1007/s00710-016-0476-9

ORIGINAL PAPER

Petrography and geochemistry characteristics of the lower Cretaceous Muling Formation from the Laoheishan Basin, Northeast China: implications for provenance and tectonic setting

Yu Song[1,2] · **Zhaojun Liu**[1,2] · **Qingtao Meng**[1,2] · **Yimeng Wang**[1,2] · **Guodong Zheng**[1,2] · **Yinbo Xu**[3]

Received: 7 January 2016 / Accepted: 25 August 2016 / Published online: 20 October 2016

Abstract The petrography, mineralogy and geochemistry of sedimentary rocks from the lower Cretaceous Muling Formation (K_1ml) in the Laoheishan basin, northeast (NE) China are studied to determine the weathering intensity, provenance and tectonic setting of the source region. Petrographic data indicate the average quartz-feldspar-lithic fragments (QFL) of the sandstone is Q = 63 %, F = 22 %, and L = 15 %. Lithic fragments mainly contain volcanic clasts that derived from surrounding basement. X-ray diffraction (XRD) data reveal abundant clay and detrital minerals (e.g. quartz), as well as minor calcite in the fine-grained sediments. The Hf contents and element concentration ratios such as Al_2O_3/TiO_2, Co/Th, La/Sc, and La/Th are comparable to sediments derived from felsic and intermediate igneous rocks. The strong genetic relationship with the igneous rocks from the northwest and northeast areas provides evidence that the sediments of the Muling Formation (K_1ml) in the Laoheishan basin have been derived from this area. The chemical index of alteration (CIA) and index of chemical variability (ICV) reveal an intensive weathering in the source region of the sediments. The multidimensional tectonic discrimination diagrams indicate that the source rocks of K_1ml are mainly derived from the collision system. However, they may also comprise sediments derived from the continental rift system. The results are consistent with the geology of the study area.

Keywords Provenance · Tectonic setting · Petrography · Geochemistry · Laoheishan basin · Northeast China

Editorial handling: M. A.T.M. Broekmans

✉ Zhaojun Liu
liuzj@jlu.edu.cn

[1] College of Earth Sciences, Jilin University, Changchun 130061, China

[2] Key Laboratory for Oil Shale and Paragenetic Energy Minerals, Jilin University, Changchun 130061, China

[3] Oil and Gas Resources Strategic Research Center, Ministry of Land and Resources, Beijing 100034, China

Introduction

The geochemical composition of clastic sediments has been widely used to decipher the provenance (Madhavaraju and Lee 2010; Migani et al. 2015; Odoma et al. 2015), to evaluate the weathering history of the source area (Zaid 2013; Rahman et al. 2014), and to infer the tectonic settings (Roser and Korsch 1986; Armstrong-Altrin 2015). The geochemical characteristics of clastic sediments are controlled by several factors, such as the source rock composition, weathering intensity, sedimentation and post-depositional diagenesis (Nesbitt and Young 1982; McLennan 1989). Recent studies (Armstrong-Altrin et al. 2014; Zhang et al. 2014) indicated that trace elements like Y, Sc, Th, Zr, Hf, Cr, Co and rare earth elements (REE) are only negligible affected by chemical weathering, denudation, and aggradation. Therefore, these elements can be used to in provenance studies and to determine the tectonic settings of sedimentary basins (Cullers et al. 1987; Condie et al. 1992; Holail and Moghazi 1998; McCann 1998). However, because of multiple factors controlling the geochemical characteristics of sedimentary rocks, combined petrological and geochemical analyses should be applied to reveal the provenance and tectonic setting of a sedimentary basin (Hanson et al. 2001; Zhang et al. 2012; Xu et al. 2013a, b).

The Laoheishan basin is located in the eastern Heilongjiang Province, northeast China (Fig. 1), and contains abundant coal and oil shale resources. Previous studies were focused only on the calculation of coal resources, the provenance and tectonic

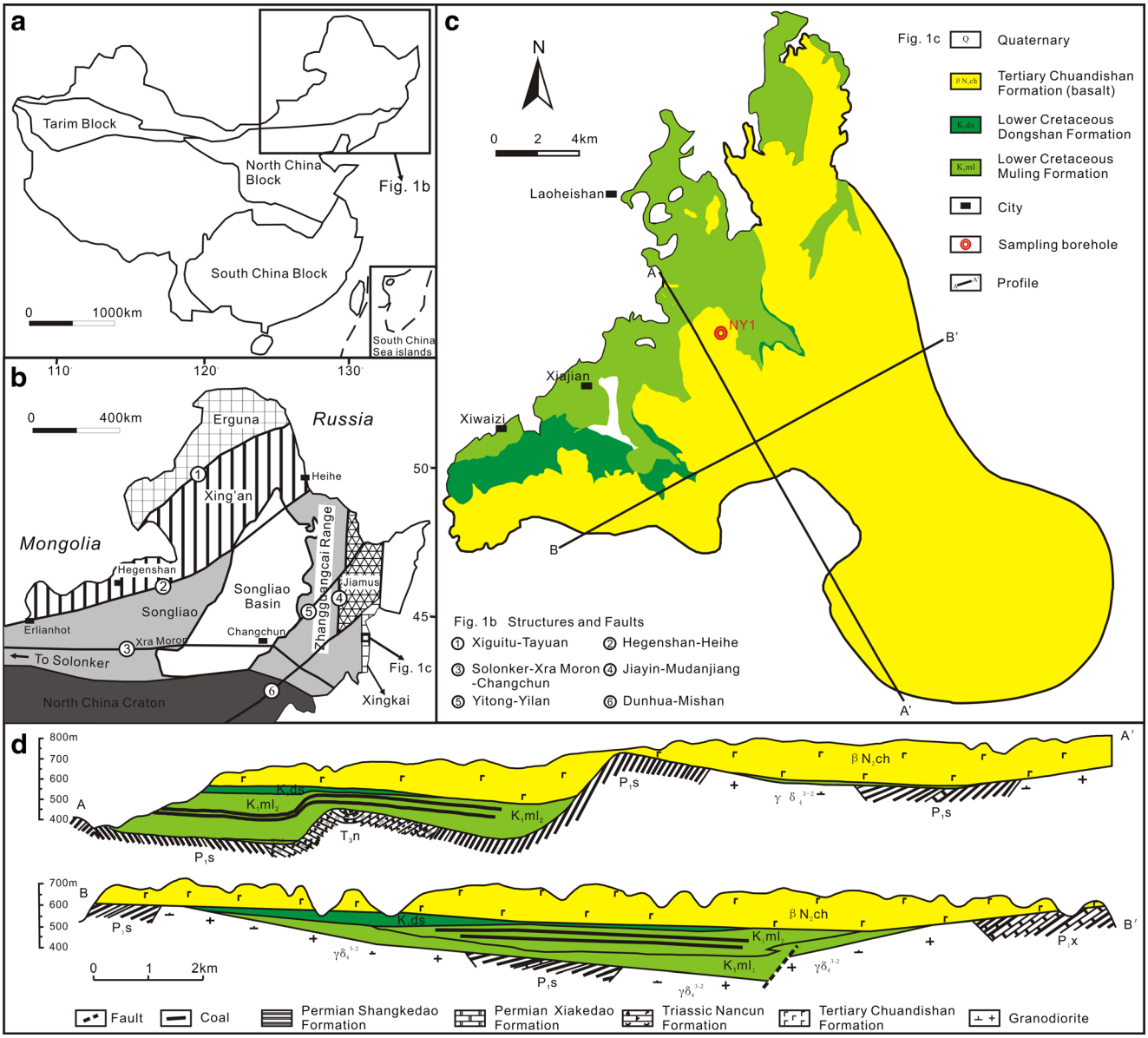

Fig. 1 **a** Sketch map showing the geotectonic of China (Lv et al. 2015), **b** tectonic units of northeast China showing the position of the Xingkai massif (Wu et al. 2007; Xu et al. 2012), **c** geological map of the Laoheishan basin and the sampling location, **d** profiles of the Laoheishan basin showing the basin structure

setting of clastic sediments has not been studied. In this study, the petrological and geochemical analyses are carried out on the clastic sediments of the Muling Formation to infer paleoweathering, source rock characteristics, and tectonic setting.

Geological setting

Northeast China is formed by several micro-continental blocks separated by major faults. The micro-continental blocks are (from NW to SE) the Erguna, Xing'an, Songliao, Jiamusi and Xingkai blocks (Fig. 1a, b) (Wu et al. 2007).

The Laoheishan basin is situated in the Xingkai Block composed of Precambrian metamorphic basement, partly covered by carbonate, clastic and volcanic rocks of Paleozoic and Mesozoic age (Shi 2006; Xu et al. 2012). The basin covers an area of approximately 400 km^2. Outcrops of the Cretaceous basin fill are very rare and occur only in northwestern part of the basin (Fig. 1c). The central and southeastern parts of the basin are covered by extensive and thick basalt layers of the Tertiary Chuandishan Formation (Fig. 1c, d).

The Lower Cretaceous basin fill is about 400 m thick and dips southeastwards with less than 5°. It comprises the Muling Formation and the overlying Dongshan Formation. The Muling Formation is subdivided into two members. The lower

member is composed of conglomerate with interbedded sandstone and mudstone (K_1ml_1). In contrast, the upper member (K_1ml_2) consists of mudstone, sandstone and limited conglomerate, with several coal and oil shale layers (Fig. 2).

Samples and analytical methods

Samples for the study were collected from the new-drilled well NY1, which located in the basin center (Fig. 1c) with large thickness of K_1ml (total thickness 277.22 m). The samples were taken in K_1ml_2 (total thickness 263.46 m), from 121 to 372.8 m interval and the sample location was indicated in Fig. 3. Twenty-four sandstone samples have been selected for petrographic study (Fig. 3; Table 1) and 8 fine-grained sediments (Fig. 3; Table 2) were analyzed for the mineral composition. Additionally, 11 (Fig. 3; Table 3) and 35 fine-grained sediments (Fig. 3; Tables 4 and 5) have been selected for major elements, trace and rare earth elements analyses, respectively. For mineral composition and geochemical analyses, samples were ground in an agate mortar and stored in the glass capillary to prevent oxidation prior to analysis.

For petrographic investigations, 24 thin sections were prepared following the procedure by Camuti and McGuire (1999). The point counts were done using Dickinson (Dickinson, 1985) and standard methods. In each section, we used the 300-grain-count practice originally from Dryden (1931), for total quartz [Q = monocrystalline quartz (Qm) + polycrystalline quartz (Qp)], total feldspar [F = K-feldspar (K) + plagioclase feldspar (P)] and total lithic fragments [L = volcanic (Lv) + sedimentary (Ls) + metamorphic (Lm) rock fragments] (Dickinson 1970; Ingersoll et al. 1984), the results were presented in Table 1. The mathematical background for point-counting statistics is shown in Howarth (1998), and the statistical error is ±5 vol%. The practical procedures are given in Howarth and French (1998).

X-ray diffraction analyses were conducted on a Philips PW 1830/40 device using CuKα-radiation (1.54 Å, 35 kV, 35 mA). Scans with a step size of 0.02° were run between 2 and 67° 2θ in the air-dry state (random powder mount and oriented powder mount) and between 2 and 45° 2θ in the ethylene- glycoliated state and after heating to 350 and 550° C. Qualitative processing was done using the dataset of Brindley and Brown (1980) and Moore and Reynolds (1997). Quantitative interpretation was carried out using the methods described by Schultz (1964).

The major element compound content was determined using a Philips PW2404 X-ray fluorescence (XRF) spectrometer. Powdered samples were heated to 110° C for 6 h followed by heating in a muffle furnace at 1000° C for two hours to determine LOI (loss on ignition). Lithium tetraborate was mixed with the samples and heated to 1000° C to form a fused samples for XRF analysis. An international reference standard material (JB-2) was used to check the accuracy that was better than ±5 % and the precision of the measurement based on

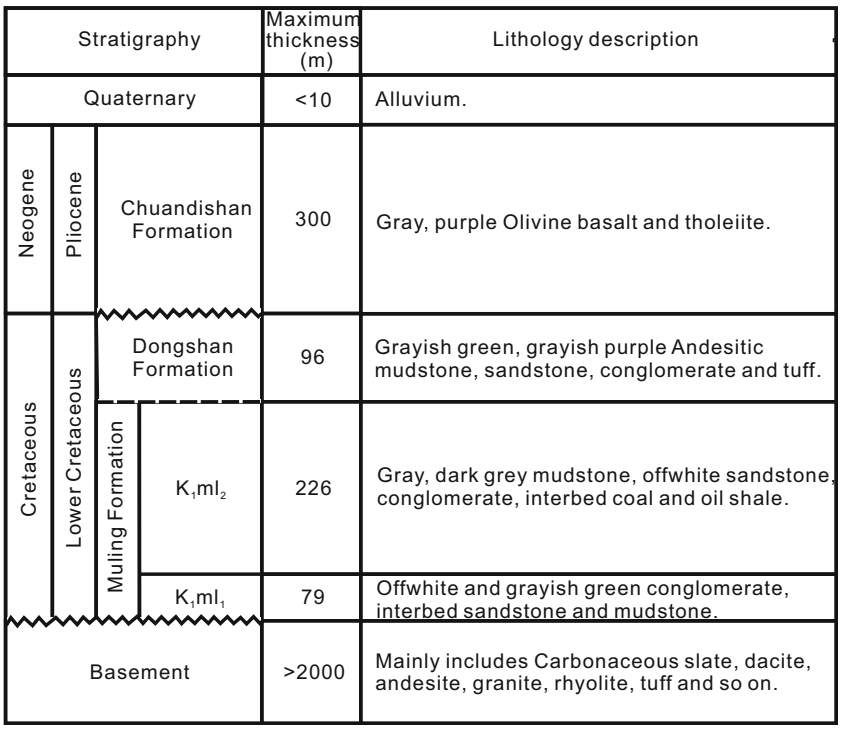

Fig. 2 Stratigraphic division of the Laoheishan basin

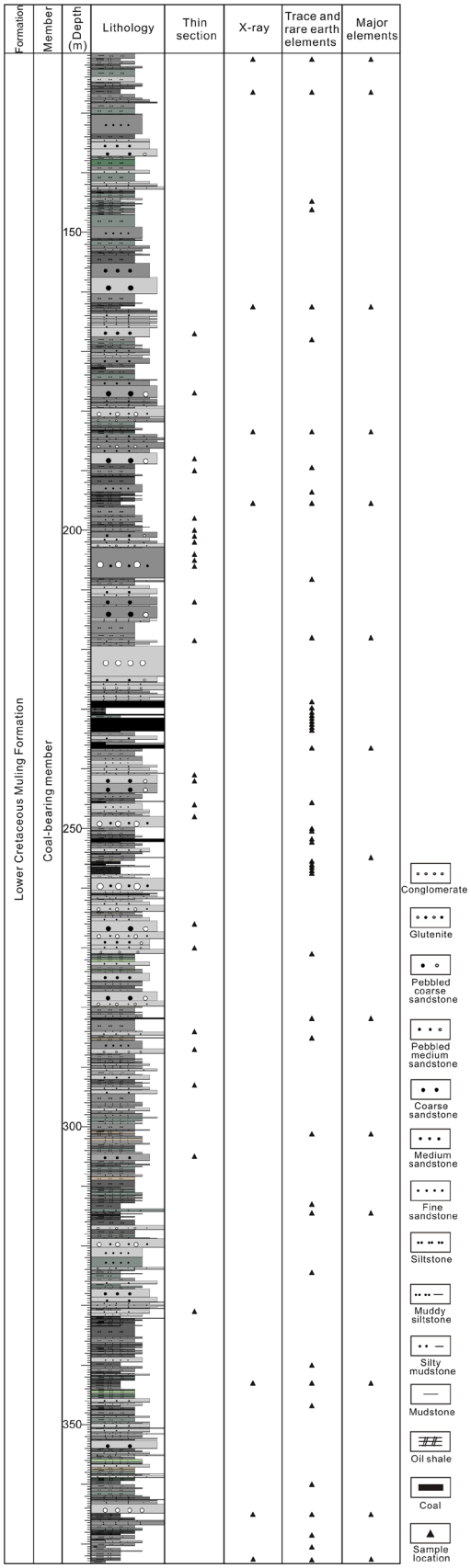

Fig. 3 Lithologic log of well NY-1, visualizing sampling depth and principal investigations performed

duplicate was within the acceptable limit. The results are reported in Table 3, CIA refers to the chemical index of alteration, which proposed by Nesbitt and Young (1982), defined as $CIA = 100 \times Al_2O_3 / (Al_2O_3 + CaO^* + Na_2O + K_2O)$, and CaO* refers only to the CaO in siliceous minerals. ICV refers to the index of chemical variability, proposed by Cox et al. (1995), defined as $ICV = (Fe_2O_3 + K_2O + Na_2O + CaO + MgO + MnO + TiO_2)/Al_2O_3$.

Trace and rare earth elements were determined from solutions prepared by homogenized samples powder dissolved in reagent grade HF: HNO_3 acid mixture in screwtop vessels. A test portion (0.05 g) of samples was added to 25 ml pressure decomposition vessels. Matrix matching international certified reference materials MAG-1 (marine mud, United States) and GSR-4 (sandstone sediment, China) along with couple of procedural blanks were also prepared with the sample batch by adopting the same protocol described above to negate errors due to reagent and handling. Solutions were analyzed by high resolution inductively coupled plasma mass spectrometer (HR-ICP-MS) (Thermo Scientific X-Series). The MAG-1 was used for calibration. The analytical precision for all the elements was estimated to be <5 % based on duplicate analyses of samples and standards. The results are reported in Tables 4 and 5.

Results

Petrography

The sandstones from the lower Cretaceous Muling Formation comprise three components: framework gains, cements, and pores. Most of the framework grains are medium sorted, subangular to sub-round in shape and are texturally moderately mature (Armstrong-Altrin et al. 2015b), mainly composed of quartz (Q), feldspar (F) and rock fragments (L), with a few heavy minerals and matrix (Table 1). The average ratio of Q-F-L is Q_{63}-F_{22}-L_{15}, indicate the compositionally moderately mature.

Quartz is the most abundant grain component in the sandstones and can be subdivided into two groups: monocrystalline quartz (Qm) and polycrystalline quartz (Qp) (Table 1; Fig. 4a, b). Qm contains nonundulose and undulose grains, indicating low-grade metamorphism (Basu et al. 1975); and most Qp grains consist of more than three crystals of two types: 1) more than five elongated irregular crystals with crenulated intercrystal boundaries (Fig. 4a); 2) five or more crystals with straight to slightly curved inter-crystals boundaries (Fig. 4b). The first type indicating a metamorphic origin (Asiedu et al. 2000) is less in the study area, whereas the second type is predominant, indicating an igneous origin (Tucker 2009).

Table 1 Modal point-count data of sandstone samples from the Laoheishan basin

Sample	Depth (m)	Granularity*	Qm (vol%)	Qp	Q	K	P	F	Lv	Ls	Lm	L
NY-B-1	167	Medium	48	5	53	24	12	36	6	0	5	11
NY-B-2	177	Coarse	34	14	48	19	14	33	14	0	5	19
NY-B-3	188	Coarse	49	8	57	9	11	20	17	0	6	23
NY-B-4	190	Silt	57	5	62	17	7	24	9	0	5	14
NY-B-5	198	Fine	59	7	66	10	14	24	5	0	5	10
NY-B-6	200	Fine	65	5	70	6	14	20	5	0	5	10
NY-B-7	201	Coarse	34	18	52	15	18	33	9	0	6	15
NY-B-8	202	Coarse	60	6	66	5	11	16	13	0	5	18
NY-B-9	204	Coarse	29	15	44	14	13	27	17	5	7	29
NY-B-10	205	Coarse	26	14	40	15	23	38	14	0	8	22
NY-B-11	206	Coarse	28	17	45	9	20	29	18	0	8	26
NY-B-12	212	Coarse	61	12	73	6	9	15	7	0	5	12
NY-B-13	218.5	Medium	68	5	73	10	5	15	7	0	5	12
NY-B-14	241	Medium	54	6	60	7	9	16	16	0	8	24
NY-B-15	242	Coarse	57	7	64	9	8	17	13	0	6	19
NY-B-16	246	Fine	69	0	69	15	6	21	5	0	5	10
NY-B-17	248	Medium	73	0	73	10	6	16	6	0	5	11
NY-B-18	266	Medium	69	6	75	9	5	14	6	0	5	11
NY-B-19	270	Medium	63	5	68	12	6	18	8	0	6	14
NY-B-20	284	Fine	68	0	68	9	10	19	7	0	6	13
NY-B-21	287	Coarse	70	6	76	7	7	14	5	0	5	10
NY-B-22	293	Fine	73	0	73	6	11	17	5	0	5	10
NY-B-23	305	Medium	58	8	66	9	13	22	7	0	5	12
NY-B-24	331	Medium	68	6	74	6	7	13	7	0	6	13

Abbreviations of grain parameters (after Dickinson 1970; Ingersoll et al. 1984): Qm, monocrystalline quartz; Qp, polycrystalline quartz including chert; Q, total quartzose grains (Q = Qm + Qp); P, plagioclase feldspar; K, K-feldspar; F, total feldspar (F = P + K); Lv, volcanic rock fragments; Ls, sedimentary rock fragments; Lm, metamorphic rock fragments; L, total lithic fragments (L = Lv + Ls + Lm)

* Coarse, <2 ~ 0.5 mm; medium, <0.5 ~ 0.25 mm; fine, <0.25 ~ 0.1 mm; silt, <0.1 ~ 0.03 mm

Feldspar in the sandstones mainly comprise alkali feldspar (Fig. 4a) and plagioclase (Fig. 4d). Most feldspar grains are unaltered, although some grains are altered to sericite. Orthoclase is common in alkali feldspar, whereas microcline is very rare.

Lithic fragments in the sandstones include volcanic (Lv), sedimentary (Ls) and metamorphic (Lm) rock fragments. Volcanic rock fragments comprise felsic igneous rock (such as granite, Fig. 4c) and intermediate igneous rock (such as

Table 2 Mineralogy of the samples from the Laoheishan basin as determined by XRD

Sample	Depth (m)	Lithology	Clay minerals (wt%)					Detrital minerals (wt%)			Other mineral (wt%)
			Smectite	I/S	Illite	Kaolinite	Chlorite	Quartz	K-feldspar	Plagioclase	Calcite
NY-X-1	121	Silty mudstone	0	29	16	13	9	30	3	0	0
NY-X-2	126.5	Silty mudstone	0	19	9	10	11	32	5	14	0
NY-X-3	162.5	Silty mudstone	0	11	13	11	8	34	7	16	0
NY-X-4	183.5	Silty mudstone	26	21	9	4	3	26	3	9	0
NY-X-5	195.5	Silty mudstone	53	0	3	4	0	40	0	0	0
NY-X-6	343	Silty mudstone	0	14	5	28	11	29	5	9	0
NY-X-7	365	Mudstone	0	9	3	38	13	37	0	0	0
NY-X-8	372.8	Mudstone	0	19	3	40	9	28	0	0	1

Abbreviation: I/S, illite/ smectite mixed layer

Table 3 Major element concentrations of the samples from the Laoheishan basin as determined by XRF

Sample	Depth (m)	Lithology	$(SiO_2)_{adj}$ (wt%)	SiO_2	Al_2O_3	TFe_2O_3	CaO	Na_2O	MgO	K_2O	TiO_2	P_2O_5	MnO	LOI	Sum	CIA	ICV
NY-Z-1	121	Silty mudstone	64	58	21.3	4.7	0.8	1.8	3.1	0.4	1.03	0.03	0.02	8.20	99.50	82	0.49
NY-Z-2	126.5	Silty mudstone	64	60	18.6	6.4	1.0	2.0	3.2	1.4	1.05	0.13	0.02	6.40	99.76	71	0.63
NY-Z-3	162.5	Silty mudstone	68	63	17.9	3.7	0.9	1.6	3.5	1.6	0.82	0.13	0.02	6.90	99.57	69	0.61
NY-Z-4	183.5	Silty mudstone	68	59	16.4	3.5	1.4	2.3	2.4	1.1	0.67	0.08	0.02	13.2	99.61	73	0.58
NY-Z-5	195.5	Silty mudstone	73	60	13.4	3.4	1.0	1.3	2.1	0.5	0.78	0.02	0.01	17.6	99.61	78	0.55
NY-Z-6	218	Silty mudstone	67	63	20.8	3.2	0.8	1.3	2.9	1.4	0.78	0.03	0.02	6.00	99.82	75	0.43
NY-Z-7	301.2	Mudstone	67	59	20.5	3.0	0.6	0.9	2.4	0.9	0.82	0.05	0.01	10.9	99.61	80	0.33
NY-Z-8	314.48	Siltstone	64	45	16.0	2.8	1.2	1.1	1.7	1.3	0.56	0.10	0.01	29.9	99.50	72	0.54
NY-Z-9	343	Silty mudstone	63	58	24.8	3.6	0.6	0.9	2.5	1.0	0.78	0.05	0.02	7.90	99.70	82	0.31
NY-Z-10	365	Mudstone	65	41	16.4	2.2	1.0	0.4	1.2	0.2	0.84	0.29	0.01	35.9	99.79	89	0.35
NY-Z-11	372.8	Mudstone	60	38	19.4	1.8	0.9	0.4	1.3	0.2	0.90	0.03	0.01	36.9	99.70	90	0.28

Abbreviations: $(SiO_2)_{adj}$ volatile free SiO_2, *LOI* loss on ignition, *CIA* chemical index of alteration, *ICV* index of chemical variability

andesite, Fig. 4d); metamorphic rock fragments mainly consist of Qp; sedimentary fragments include sandstone and mudstone. The lithic fragments in the sandstones are predominantly Lv, indicating that the Muling Formation are mainly derived from igneous rock sources.

A limited content of heavy minerals is observed (<2 % on average) in the sandstones, including zircon, rutile and tourmaline. The matrix of the sandstones consist of clay minerals, carbonate, and communited lithic fragments. However, the existence of pseudomatrices makes it difficult to distinguish the primary and the epigenetic matrix (Dickinson 1970). Hence, the percentage of matrix may be overestimated.

The diagenesis of sandstones comprise compaction and cementation processes, the characteristics are as follows: 1) contact relation between detrital grains includes point and line contacts (Fig. 4); and 2) compaction deformation occurred in plastic grains (such as biotite) (Fig. 4b). The cementation mainly consist of carbonate cementation, usually formed in the primary porosity (Fig 4a).

Mineralogy

The XRD study indicates that the fine-grained sediments of K_1ml_2 mainly consist of clay minerals and detrital minerals with little other minerals (Table 2). The clay minerals on average comprise smectite (10 %), I/S mixed layers (15 %), illite (8 %), kaolinite (19 %) and chlorite (8 %). The detrital minerals comprise quartz (32 %), K-feldspar (3 %) and plagioclase (6 %), whereas the content of other mineral is very low (calcite <1 %).

Geochemistry

Major elements

Major elements concentrations in sedimentary rocks are controlled by several factors, one of the most important factors is the mineral composition (Zhang et al. 2014). For example, the K_2O/Na_2O ratio of sedimentary rocks is controlled by the relative proportion of K-feldspar to plagioclase, and the content of SiO_2 is controlled by the abundance of quartz. Furthermore, weathering can also influence the major elements concentrations in sedimentary rocks. For instance, Na in weathered crust could be carried away more easily than K, causing a strong deficit of Na and an abnormally high K_2O/Na_2O ratio; and the SiO_2 content may increase abruptly through a hydrothermal or surface weathering process (Cullers et al. 1987). The K_2O/Na_2O ratio of fine-grained sediments from the Muling Formation ranges from 0.22 to 1.18, with an average of 0.74 (Table 3), lower than the upper continental crust (UCC = 0.9), indicating these samples are

Table 4 Trace element concentrations of the samples from the Laoheishan basin as determined by HR-ICP-MS

Sample	Depth (m)	Lithology	Co (ppm)	Ni	V	Cr	Sr	Rb	Ba	Th	Sc	Nb	Ta	Zr	Hf	Y	U
NY-W-1	121	Silty mudstone	8.0	26	117	70	188	156	490	22.0	14.1	15.3	1.29	121	3.72	20.4	7.10
NY-W-2	126.5	Silty mudstone	13.3	32	98	81	216	123	500	16.1	13.0	16.0	1.27	172	5.17	26.6	4.34
NY-W-3	144.8	Silty mudstone	19.9	17	96	58	262	124	642	20.8	11.6	16.2	1.29	186	5.40	29.8	5.62
NY-W-4	146.2	Silty mudstone	32.7	28	110	42	202	65	332	9.5	12.7	18.0	0.61	714	5.17	52.2	11.8
NY-W-5	162.5	Silty mudstone	16.4	27	104	61	204	57	483	12.4	10.4	12.1	1.12	158	4.73	21.1	4.66
NY-W-6	168	Siltstone	18.7	21	61	64	305	134	708	14.2	13.2	17.8	1.40	173	5.66	26.1	2.85
NY-W-7	183.5	Argillaceous siltstone	14.7	18	75	44	399	41	452	10.4	7.1	12.5	1.19	169	5.00	16.0	4.97
NY-W-8	189.5	Argillaceous siltstone	4.0	5	31	15	621	20	591	9.5	3.8	20.4	1.09	95	3.53	13.0	3.68
NY-W-9	193.6	Silty mudstone	3.0	6	15	12	621	21	580	8.7	3.8	17.5	1.18	112	4.03	13.5	3.36
NY-W-10	195.5	Silty mudstone	1.7	8	59	43	300	108	426	12.2	8.1	17.1	0.97	121	3.36	12.2	3.13
NY-W-11	208.2	Silty mudstone	8.9	23	61	71	324	142	648	16.8	14.2	16.8	0.57	138	4.76	19.9	4.19
NY-W-12	218	Argillaceous siltstone	16.8	30	112	51	221	65	470	11.8	6.9	13.2	1.22	145	4.81	17.3	4.08
NY-W-13	230.5	Mudstone	5.7	8	141	52	215	74	364	22.8	13.5	15.7	1.48	173	5.46	23.1	6.61
NY-W-14	245.66	Mudstone	2.0	4	85	48	227	96	313	12.7	11.9	22.2	1.63	176	5.06	40.1	2.68
NY-W-15	250	Argillaceous siltstone	4.9	10	99	45	134	104	409	17.8	15.6	14.0	1.12	173	4.84	32.0	4.48
NY-W-16	250.4	Mudstone	5.8	20	175	58	239	73	389	13.9	20.0	16.7	1.09	518	6.07	27.3	3.15
NY-W-17	251.75	Mudstone	6.1	16	69	35	211	133	501	16.9	15.0	30.1	1.91	302	9.56	40.1	3.65
NY-W-18	255.5	Silty mudstone	8.8	17	84	47	177	121	471	22.1	18.7	19.1	1.51	219	6.47	39.3	6.16
NY-W-19	256	Mudstone	4.8	12	146	57	193	111	402	13.9	22.7	23.1	1.69	227	5.96	35.1	3.69
NY-W-20	256.5	Silty mudstone	14.8	16	94	41	146	99	419	18.7	14.9	21.4	1.70	296	8.31	49.2	5.41
NY-W-21	257	Silty mudstone	41.0	26	97	49	199	115	446	24.7	18.7	30.7	2.33	245	7.76	54.4	6.90
NY-W-22	257.5	Silty mudstone	5.5	8	73	42	168	94	427	18.6	14.3	31.8	2.56	396	11.1	48.1	5.34
NY-W-23	271	Argillaceous siltstone	15.3	16	146	68	197	150	436	19.1	19.2	20.1	1.52	212	5.70	40.8	6.06
NY-W-24	301.2	Mudstone	27.3	32	75	46	181	54	352	5.5	6.7	19.6	1.54	251	7.76	13.7	4.76
NY-W-25	313	Silty mudstone	15.5	25	43	20	551	60	649	6.7	5.0	8.1	0.55	113	3.87	10.8	2.35
NY-W-26	314.48	Siltstone	7.1	20	72	24	412	60	467	8.3	6.1	18.2	0.67	148	3.04	11.4	2.72
NY-W-27	324.5	Silty mudstone	18.4	16	107	70	314	169	609	19.5	15.6	22.7	1.55	190	5.89	33.4	9.58
NY-W-28	340	Silty mudstone	6.1	11	87	56	307	131	634	14.1	12.1	19.0	1.28	157	4.68	25.8	3.48
NY-W-29	343	Silty mudstone	6.4	14	85	48	110	38	234	6.8	5.3	15.1	1.34	169	5.83	10.4	2.55
NY-W-30	346.8	Silty mudstone	24.1	27	116	60	151	123	419	15.2	18.7	14.5	1.08	299	8.17	46.5	5.87
NY-W-31	360	Silty mudstone	9.6	14	119	53	100	107	426	17.2	19.1	13.6	1.05	190	5.30	25.9	2.84
NY-W-32	365	Mudstone	2.8	13	148	64	125	39	183	6.4	15.0	9.4	0.73	222	5.92	38.9	2.40
NY-W-33	368.5	Mudstone	14.6	16	133	79	113	86	295	12.1	20.3	15.9	1.14	327	7.42	41.8	4.52
NY-W-34	370.5	Mudstone	6.6	15	108	70	86	69	230	10.7	21.2	14.8	1.01	396	9.55	39.4	8.59
NY-W-35	372.8	Mudstone	10.1	17	202	64	81	94	147	10.6	8.2	12.1	1.10	436	8.67	29.5	17.05
		UCC	10.0	20	60	35	350	112	550	10.7	11.0	25.0	2.20	190	5.80	22.0	2.80

Abbreviation: *UCC* upper continental crust, data from Taylor and McLennan (1985)

affected by weathering. The medium content of SiO_2 (38 ~ 63 %, with an average of 55 %) indicates medium mineral maturity and medium content of quartz and/or Si-rich minerals (Zhang et al. 2014). The relatively high ferromagnesian element concentrations (such as TiO_2, Fe_2O_3, and MgO) indicate some influence from basic rocks. The high Al_2O_3 content (13.4 ~ 24.8 %, with an average of 18.7 %) is probably related to the high content of aluminum-rich minerals, such as clay minerals, feldspar and mica.

Trace elements

The selected trace elements are discussed as three groups, i.e. transition trace elements (TTE: Co, Ni, V, Cr), large ion lithophile elements (LILE: Sr, Rb, Ba) and high field strength elements (HFS: Th, Sc, Nb, Ta, Zr, Hf, Y, U). Table 4 lists the selected trace elements concentrations, the distribution pattern of these elements are presented in Fig. 5.

The TTE in fine-grained sediments are enriched relative to the upper continental crust (UCC), indicating a cryptic mafic

Table 5 Rare earth element concentrations of the samples from the Laoheishan basin as determined by HR-ICP-MS

Sample	Lithology	La (ppm)	Ce	Pr	Nd	Sm	Eu	Gd	Tb	Dy	Ho	Er	Tm	Yb	Lu	ΣREE	ΣLREE/ ΣHREE	$(La/Yb)_N$	δEu
NY-W-1	Silty mudstone	39.53	75.81	9.34	33.77	6.39	1.29	5.31	0.74	4.23	0.78	2.27	0.34	2.10	0.31	182.22	10.32	13.32	0.66
NY-W-2	Silty mudstone	35.73	69.23	8.56	32.80	6.42	1.38	5.96	0.88	5.18	1.03	2.99	0.44	2.90	0.41	173.91	7.79	8.72	0.66
NY-W-3	Silty mudstone	54.40	102.00	12.40	48.20	8.90	1.92	6.93	1.18	6.04	0.99	3.09	0.44	2.87	0.44	249.80	10.36	13.43	0.72
NY-W-4	Silty mudstone	28.60	52.60	6.46	25.90	5.45	1.39	5.49	1.36	7.98	1.67	5.16	0.79	5.63	0.75	149.22	4.18	3.60	0.75
NY-W-5	Silty mudstone	32.29	67.84	8.49	32.79	6.59	1.46	6.02	0.81	4.73	0.89	2.52	0.36	2.40	0.33	167.52	8.28	9.53	0.69
NY-W-6	Siltstone	40.10	78.80	9.58	37.40	7.01	1.55	5.61	1.01	5.19	0.89	2.66	0.40	2.79	0.33	193.32	9.24	10.18	0.73
NY-W-7	Argillaceous siltstone	26.65	51.53	6.34	23.52	4.66	0.93	4.20	0.57	3.40	0.66	1.92	0.30	1.89	0.28	126.86	8.59	9.97	0.62
NY-W-8	Argillaceous siltstone	29.20	54.60	6.06	21.20	3.78	0.66	3.12	0.54	2.61	0.46	1.32	0.20	1.12	0.17	125.04	12.12	18.47	0.57
NY-W-9	Silty mudstone	25.10	48.90	5.46	19.00	3.25	0.55	2.79	0.46	2.44	0.42	1.28	0.21	1.42	0.22	111.50	11.07	12.52	0.54
NY-W-10	Silty mudstone	14.79	27.20	3.02	10.67	1.96	0.42	1.83	0.27	1.94	0.43	1.43	0.24	1.65	0.25	66.09	7.23	6.34	0.65
NY-W-11	Silty mudstone	39.70	73.30	8.83	33.70	6.23	1.41	4.99	0.85	4.33	0.76	2.31	0.33	2.13	0.33	179.20	10.18	13.20	0.75
NY-W-12	Argillaceous siltstone	22.03	48.99	5.78	21.99	4.59	0.95	4.33	0.64	3.90	0.76	2.32	0.33	2.28	0.32	119.20	7.02	6.84	0.63
NY-W-13	Mudstone	27.80	50.20	6.22	24.20	5.06	0.91	4.58	0.87	4.82	0.92	2.68	0.42	2.73	0.41	131.82	6.56	7.21	0.56
NY-W-14	Mudstone	26.60	47.40	5.51	21.20	4.08	0.84	3.83	0.92	5.79	1.32	4.16	0.72	4.92	0.75	128.04	4.71	3.83	0.63
NY-W-15	Argillaceous siltstone	39.40	78.10	9.25	35.50	6.77	1.31	6.18	1.09	5.74	1.10	3.31	0.56	3.72	0.57	192.60	7.65	7.50	0.60
NY-W-16	Mudstone	14.70	24.00	3.29	12.40	2.50	0.57	2.53	0.55	3.87	0.90	3.08	0.57	4.08	0.73	73.76	3.53	2.55	0.67
NY-W-17	Mudstone	60.00	102.00	12.20	46.80	8.49	1.07	7.22	1.29	7.33	1.40	4.31	0.74	4.89	0.75	258.49	8.25	8.69	0.40
NY-W-18	Silty mudstone	58.10	109.00	12.80	48.70	8.92	1.62	7.72	1.33	7.00	1.27	3.96	0.64	4.26	0.62	265.93	8.93	9.66	0.58
NY-W-19	Mudstone	31.30	57.90	7.21	29.00	6.10	1.30	5.54	1.18	6.60	1.29	3.94	0.69	4.89	0.76	157.70	5.34	4.53	0.66
NY-W-20	Silty mudstone	57.00	106.00	12.60	49.60	9.32	1.53	8.21	1.45	7.86	1.55	4.64	0.74	4.92	0.75	266.17	7.84	8.21	0.52
NY-W-21	Silty mudstone	61.10	123.00	14.20	55.30	10.80	1.72	9.45	1.75	9.53	1.89	5.66	0.92	5.98	0.91	302.20	7.38	7.24	0.50
NY-W-22	Silty mudstone	38.30	79.50	9.35	37.00	7.23	1.01	6.65	1.31	7.69	1.61	5.16	0.89	6.01	0.94	202.65	5.70	4.51	0.43
NY-W-23	Argillaceous siltstone	58.70	105.00	13.00	52.00	9.57	1.89	8.57	1.57	8.44	1.58	4.43	0.73	4.79	0.70	270.96	7.80	8.68	0.62
NY-W-24	Mudstone	17.40	44.53	5.09	19.50	4.18	0.67	3.94	0.64	4.33	0.91	2.92	0.46	3.11	0.45	108.13	5.45	3.96	0.49
NY-W-25	Silty mudstone	25.10	51.20	5.86	22.60	3.69	0.90	3.02	0.46	2.07	0.35	1.01	0.14	0.94	0.15	117.48	13.44	19.02	0.80
NY-W-26	Siltstone	19.26	36.83	4.23	15.53	2.92	0.75	2.59	0.33	2.08	0.40	1.20	0.19	1.20	0.18	87.68	9.75	11.39	0.81
NY-W-27	Silty mudstone	56.20	112.00	13.20	51.80	9.60	1.89	7.63	1.29	6.48	1.22	3.39	0.52	3.58	0.51	269.31	9.94	11.12	0.65
NY-W-28	Silty mudstone	46.20	87.60	10.30	39.70	7.20	1.52	6.00	1.00	5.27	0.90	2.73	0.39	2.43	0.34	211.58	10.10	13.47	0.68
NY-W-29	Silty mudstone	10.45	26.75	3.08	12.21	2.62	0.54	2.56	0.39	2.59	0.54	1.74	0.28	1.95	0.29	65.99	5.39	3.79	0.62
NY-W-30	Silty mudstone	66.60	140.00	15.80	64.20	12.40	2.49	10.60	1.79	9.22	1.68	4.99	0.78	5.46	0.80	336.81	8.54	8.64	0.64
NY-W-31	Silty mudstone	39.20	77.10	8.92	34.30	6.22	1.30	5.38	0.92	4.89	0.95	2.81	0.46	3.20	0.50	186.15	8.74	8.68	0.66
NY-W-32	Mudstone	17.74	38.56	4.54	19.11	5.02	1.24	6.52	1.13	7.61	1.66	4.73	0.67	4.08	0.60	113.21	3.19	3.08	0.64
NY-W-33	Mudstone	25.10	50.70	6.25	24.90	5.21	1.08	4.82	1.05	6.89	1.35	4.10	0.75	4.82	0.71	137.72	4.63	3.69	0.64
NY-W-34	Mudstone	17.20	31.50	4.16	17.20	3.75	0.82	4.23	0.97	6.18	1.31	3.99	0.67	4.49	0.70	97.17	3.31	2.71	0.61
NY-W-35	Mudstone	34.00	69.52	9.39	36.01	7.58	1.46	6.89	1.10	6.89	1.36	3.84	0.53	3.41	0.48	182.46	6.45	7.07	0.60
	Chondrite	0.24	0.61	0.10	0.47	0.15	0.06	0.21	0.04	0.25	0.06	0.17	0.03	0.17	0.03	2.59	1.70		

$(La/Yb)_N$, ratio of La_N and Yb_N, La_N and Yb_N are chondrite-normalized values

$\delta Eu = Eu_N/(Sm_N X Gd_N)^{1/2}$, Eu_N, Sm_N and Gd_N are chondrite-normalized values

Chondrite data from Taylor and McLennan (1985)

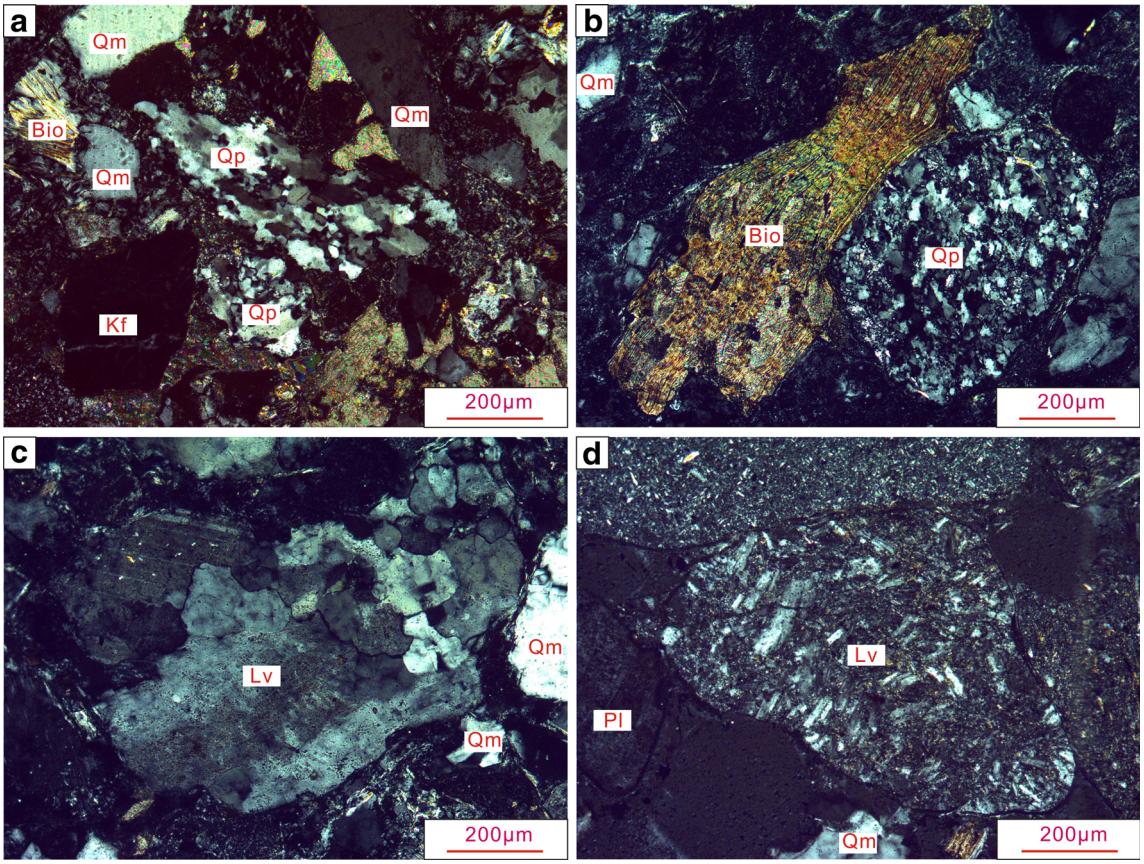

Fig. 4 Photomicrographs of the Muling Formation sandstone samples (cross-polarized light): **a** Qp grains belonging to metamorphic rock fragments, along with K-feldspar (Kf), Qm, biotite (Bio) grains and carbonate cement (Cc); **b** Qp grain belonging to igneous rock fragment, Qm and biotite (Bio) grain; **c** acid igneous rock fragment (Lv, probably granite fragment) and Qm grains; **d** intermediate igneous rock fragment (Lv, probably andesite fragment) along with plagioclase (Pl) and Qm grains

or ultramafic component carried in the clay fractions of the sediments (Hossain et al. 2010). The LILE are depleted relative to the UCC. Among these, Rb shows the greatest depletion (Fig. 5). Because Rb is incorporated into clay during chemical weathering (Nesbitt and Young 1982), so it indicates strong chemical weathering in the source area. The HFS are similar to the UCC, suggesting the source rocks are probably derived from the UCC (McLennan et al. 1995).

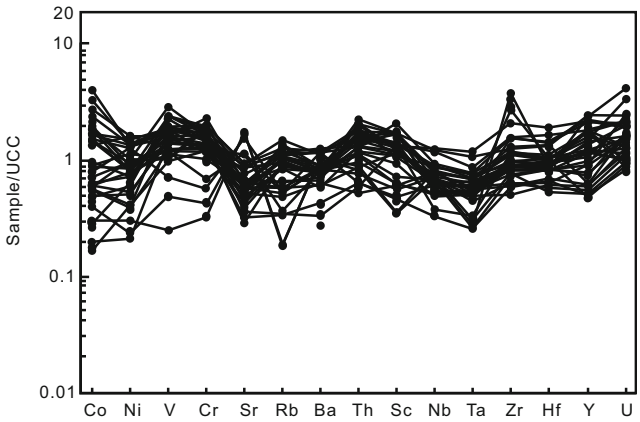

Fig. 5 UCC-normalized selected trace elements diagram of samples from the Laoheishan basin (UCC data from Taylor and McLennan 1985)

Rare earth elements

The REE contents of the fine-grained sediments from the Muling Formation are presented in Table 5. The REE contents range from 65.99 to 336.81 μg/g, with an average of 171.65 μg/g, similar to the UCC (ΣREE = 146.4 μg/g), indicating a probably felsic source from the UCC (Taylor and McLennan 1985), and probably influenced by some intermediate rock sources. Of these, the total light rare earth elements (ΣLREE, include La to Eu) and total heavy rare earth elements (ΣHREE, include Gd to Lu) are 55.65–301.49 ppm and 8.03–36.08 ppm, respectively. The ΣLREE/ΣHREE ratio ranges from 3.19 to 13.44 with an average of 7.68 (Table 5). The chondrite normalized REE patterns (Fig. 6) show LREE enrichment and relatively flat HREE. The medium $(La/Yb)_N$ value (2.55–19.02, avg. 8.44) indicates the medium extent of fractionation between LREEs and HREEs, consistent with the medium ΣLREE/ΣHREE ratio. Eu anomaly (δEu) value varies between 0.40 and 0.81, with an average of 0.63, reveals a negative Eu anomaly.

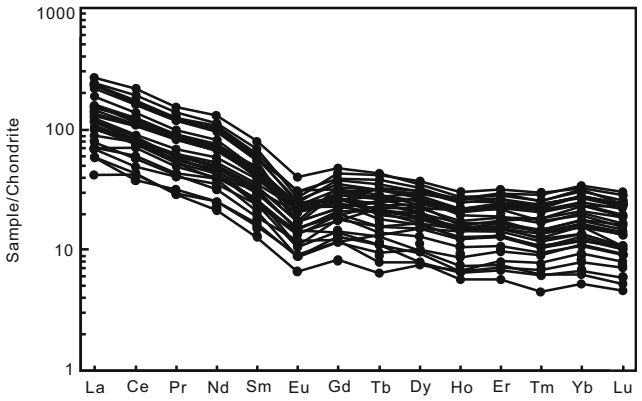

Fig. 6 Chondrite-normalized REE distributions of samples from the Laoheishan basin (Chondrite data from Taylor and McLennan 1985)

Discussion

Weathering and sediment maturity

During the weathering process, stable cations (such as Al^{3+} and Ti^{4+}) are sorted in stable weathering products, whereas the unstable cations (such as Na^{+}, Ca^{2+} and K^{+}) tend to be lost (Fedo and Nesbtit 1995). Such elemental enrichment and loss commonly depend on the intensity of chemical weathering (Condie et al. 1992). In order to quantify the degree of weathering, Nesbitt and Young (1982) proposed the Chemical Index of Alteration (CIA). The Al_2O_3-(Na_2O + CaO*)-K_2O ternary diagram (Fig. 7) shows that the CIA of K_1ml_2 samples range from 69 to 90 with an average of 78, suggesting strong chemical weathering.

The index of chemical variability (ICV; Cox et al. 1995) is a measure to identify the compositional maturity of sediments, which has successfully applied in many studies (Armstrong-Altrin et al. 2015a, b). Typical rock forming minerals like feldspars, amphiboles, and pyroxenes have ICV values of >1, whereas alteration products such as kaolinite, illite, and muscovite have ICV values <1 (Cox et al. 1995; Cullers and Podkovyrov 2000). The ICV values of K_1ml_2 samples range from 0.28 to 0.63 with an average of 0.47, indicating the samples are geochemically moderately mature and may derive from a strong weathered source.

Provenance

The sedimentary source regions

The sandstones from the Muling Formation show medium to high quartz content, relatively low contents of feldspar and lithic fragments (Table 1), medium sorted, and sub-angular to sub-round in shape. These features are indicative of compositionally and texturally moderately mature. The types of lithic fragments in sandstones are similar to the basement surrounding the basin. Furthermore, in conglomerates at the K_1ml_1, much gravel has been found from the basement, i.e. dacite, acid tufflava, andesite, granite, rhyolite and tuff, etc., suggesting the felsic and intermediate igneous source rocks. Dickinson (1985) suggested that detrital modes of sandstone suites primarily reflect the different tectonic settings of provenance terranes. On the Q-F-L ternary diagram, most of the K_1ml_2 sandstones plot in the recycled orogeny field (Fig. 8).

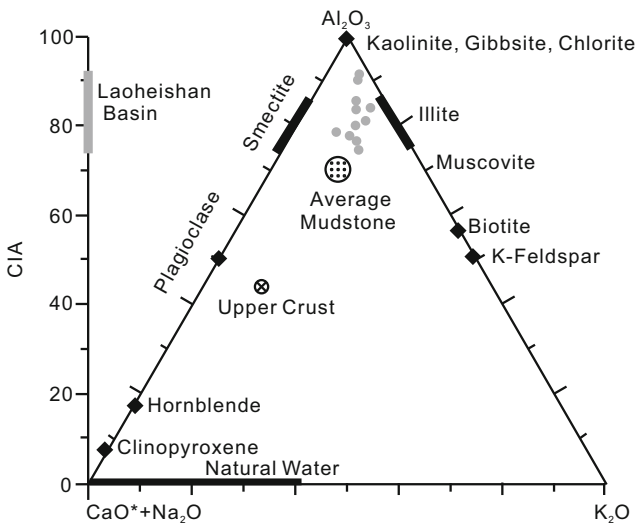

Fig. 7 Al_2O_3-(Na_2O + CaO*)-K_2O ternary diagram of samples from the Laoheishan basin, showing the weathering status of its source rocks (after Condie et al. 1992)

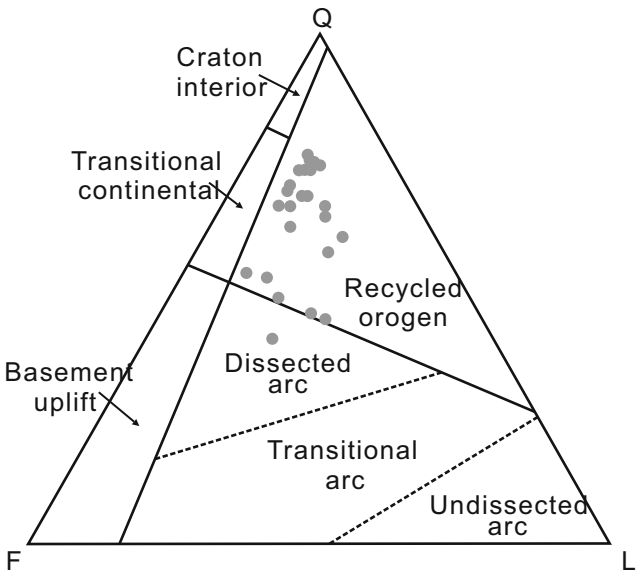

Fig. 8 Q-F-L ternary plots from the Muling Formation sandstone in the Laoheishan basin (Q = Quartz; F = feldspar; L = lithic rocks) (after Dickinson 1985)

Type of the source rocks

Major and trace element concentrations of terrigenous sediments can give a reliable clue about the provenance of the source area (Armstrong-Altrin et al. 2015b; Odoma et al. 2015). Among major elements, Al_2O_3 and TiO_2 are considered as immobile during weathering, transportation, and diagenesis. Hence, the Al_2O_3/TiO_2 ratio can be used to infer the source rock composition (Zhou et al. 2015). According to Hayashi et al. (1997), the Al_2O_3/TiO_2 ratios range from 3 to 8 represent mafic, 8–21 indicate intermediate and 21–70 for felsic igneous rocks. The Al_2O_3/TiO_2 ratios of fine-grained samples from the K_1ml_2 vary between 17 and 32. The variation in Al_2O_3/TiO_2 ratios indicate that K_1ml_2 samples are derived from felsic and intermediate igneous source rocks.

Trace elements such as Sc, Ni, Cr and Co tend to be enriched in mafic rocks, whereas La, Th, Hf, Zr and REE are richer in acidic rocks (Cullers and Podkovyrov 2000). The fine-grained sediments from K_1ml_2 show variable La/Sc ratio (0.81–7.68, avg. 3.04) and relatively constant Co/Th ratio (0.14–4.96, avg. 0.97), which plot mostly in felsic volcanic rock and andesite areas (Fig. 9a). Floyd and Leveridge (1987) established a discrimination diagram using the La/Th ratio vs. Hf to determine different sources and to further distinguish the andesite and basalt sources. The samples show relatively low La/Th ratio (<5.0) and Hf content (3.04–11.1, avg. 5.94), suggesting that they may have originated from felsic and intermediate source rocks (Fig. 9b). Thus, the geochemical analyses indicate that the source rocks of the K_1ml are mainly derived from felsic and intermediate igneous rocks, probably felsic volcanic rock and andesite.

The location of source area

Several igneous rocks developed surrounding the Laoheishan basin, such as the northwestern granodiorite, the northeastern quartz diorite, the northern granite porphyry and the pyroxene diorite (Cheng et al. 2006; Zhao et al. 2009; Xu et al. 2013a, b). Previous studies indicated that the granodiorite from the northwest is strong REE fractionation ($(La/Yb)_N = 6.34–16.68$) with a negative Eu anomaly ($\delta Eu = 0.53–0.74$) (Zhao et al. 2009), similar to the K_1ml_2 samples (Fig. 10a). Similarly, the quartz diorite from the northeast also shows relatively strong REE fractionation ($(La/Yb)_N = 5.28–8.21$) and a negative Eu anomaly ($\delta Eu = 0.63–0.82$) (Zhao et al. 2009; Fig. 10b). However, the granite porphyry from the north reveals strong REE fractionation ($(La/Yb)_N = 8.29$) with a weak positive Eu anomaly ($\delta Eu = 1.07$) (Xu 2009; Fig. 10c), and the pyroxene diorite from the north suggests weak REE fractionation and a weak positive Eu anomaly (Zhao 2013; Fig. 10d), which are different from the studied samples.

Therefore the source rocks of the K_1ml_2 have strong genetic relationships with the granodiorite and quartz diorite from the northwest and the northeast, respectively. But have weak relationships with the granite porphyry and the pyroxene diorite from the north, suggesting the source rocks may contain granodiorite and quartz diorite, and probably derived from the northwest and the northeast areas.

Tectonic setting

The distinctive elemental compositions of siliciclastic rocks in various tectonic environments have been widely used to indicate the tectonic setting of their respective sedimentary basins (Bhatia 1983; Bhatia and Crook 1986). Recently, based on the geochemical composition of Neogene-Quaternary sediments,

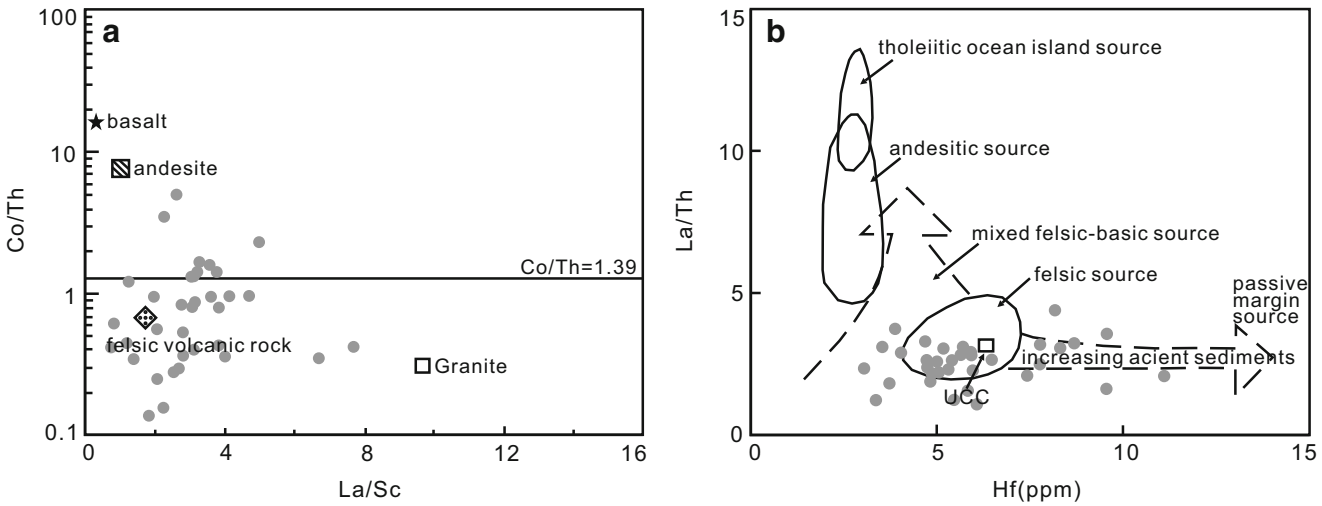

Fig. 9 Source rock discrimination diagrams for the K_1ml_2 samples in the Laoheishan basin; **a** La/Sc vs. Co/Th (after Wronkiewicz and Condie 1987); **b** Hf vs. La/Th plot (after Floyd and Leveridge 1987)

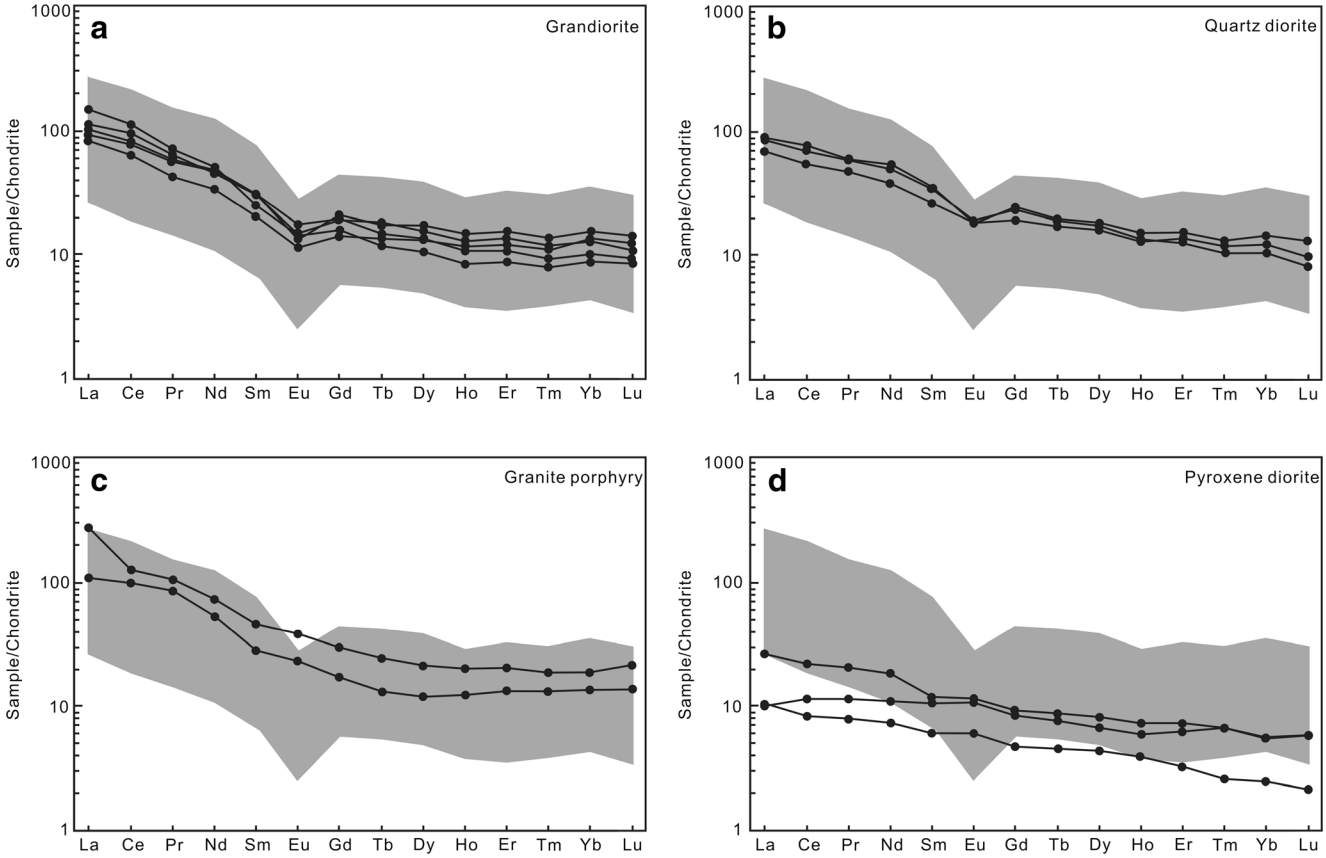

Fig. 10 Chondrite-normalised REE distribution patterns of the study area and granite surrounding the Laoheishan basin (Chondrite data from Taylor and McLennan 1985). The grey shaded zones represent the REE distribution of the K_1ml_2 samples. **a** Granodiorite in the northeastern basin, with data from Zhao et al. (2009); **b** Quartzdiorite in the northwestern basin, with data from Zhao et al. (2009); **c** Granite porphyry in the northern basin, with data from Xu (2009); **d** Pyroxene diorite in the northern basin, with data from Zhao (2013)

Verma and Armstrong-Altrin (2013) proposed two discriminant-function-based major-element diagrams for the tectonic discrimination of siliciclastic sediments for high-silica [$(SiO_2)_{adj} = 63–95$ %] and low-silica [$(SiO_2)_{adj} = 35–63$ %] types, from three main tectonic settings: island or continental arc, continental rift and collision. In addition, these diagrams are already evaluated by some researchers (Nagarajan et al. 2015; Verma and Armstrong-Altrin 2016). In these high silica and low silica multi-dimensional diagrams, the K_1ml_2 samples are plotted in the collision and continental rift fields (Fig. 11a, b).

The previous studies indicated that at the end of the Late Jurassic (~160 Ma), the lithosphere was affected by the early collision orogeny and intracontinental compressive deformation in the region of northeast (NE) China, caused a strong crustal shortening and thickening, and increased the lithosphere thickness (Cheng et al. 2006; Xu et al. 2012; Luo et al. 2014). At the middle stage of the early Cretaceous (120–130 Ma), the rapidly oblique subduction of the Paleo-Pacific plate beneath the Eurasian continent, caused the compressed and left-lateral strike-slip shearing environment in the eastern margin of the Eurasian continent (Zhou et al. 2009; Sun et al. 2010), agitated the upwelling of asthenosphere, and caused the lithospheric mantle and part of the lower crust to submergence into the asthenosphere mantle through delamination. Meanwhile the lithosphere intense thinning made asthenosphere mantle directly contact with the crust, and resulted in the large-scale magmatism and widespread development of extensional structures in the Mesozoic (Zhao et al. 2009; Liu et al. 2014). On the basis of Mesozoic volcanic rocks in NE China, Xu et al. (2013a, b) suggested the existence of late Early Cretaceous (106 ~ 133 Ma, peak age ~115 Ma) calc-alkaline volcanic rocks in the eastern Heilongjiang–Jilin provinces indicated an active continental margin setting, and the coeval bimodal volcanic rocks in the Great Xing'an Range and the Songliao Basin suggested an intracontinental extensional environment related to the low-angle subduction of the Paleo-Pacific Plate beneath the Eurasian continent. Thus, the previous studies (Sun et al. 2010; Xu et al. 2013a, b; Liu et al. 2014; Luo et al. 2014) indicated that during the late early Cretaceous, collision and continental rift settings developed in the NE China. The Laoheishan basin located in the eastern Heilongjiang Province (Fig. 1), combined with the results obtained from the discrimination diagrams, there is a high

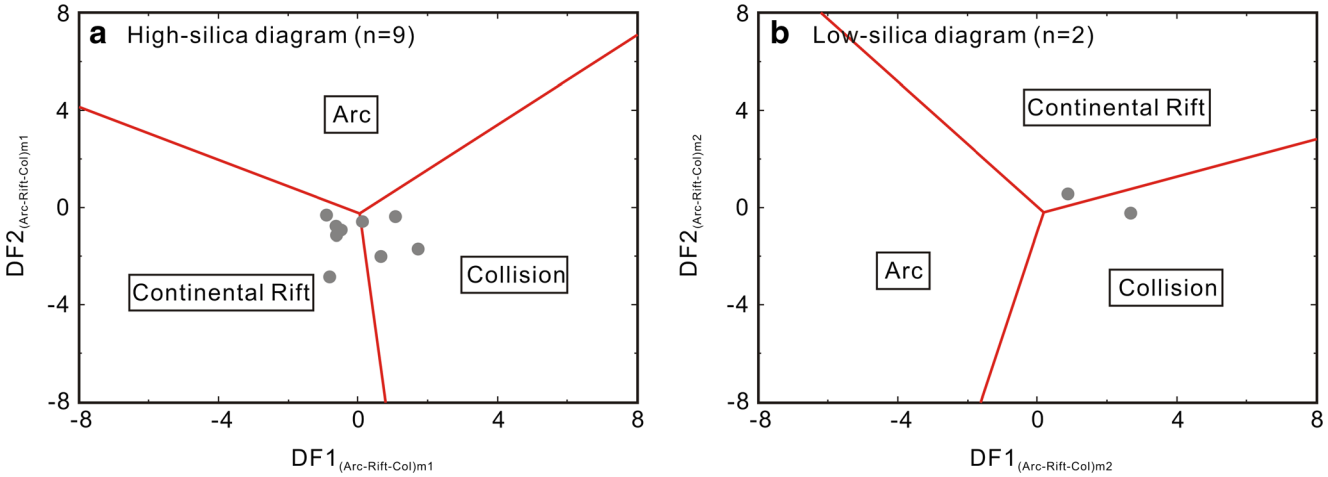

Fig. 11 Discriminant-function multi-dimensional diagram for high-silica (**a**) and low-silica (**b**) clastic sediments (Verma and Armstrong-Altrin 2013). The subscript m1 in DF1 and DF2 represents the high-silica diagram based on $\log_e$-ratios of major elements. The discriminant function equations are: (1) $DF1_{(Arc\text{-}Rift\text{-}Col)m1} = (0.263 \times \ln(TiO_2/SiO_2)_{adj}) + (0.604 \times \ln(Al_2O_3/SiO_2)_{adj}) + (1.725 \times \ln(Fe_2O_3{}^t/SiO_2)_{adj}) + (0.660 \times \ln(MnO/SiO_2)_{adj}) + (2.191 \times \ln(MgO/SiO_2)_{adj}) + (0.144 \times \ln(CaO/SiO_2)_{adj}) + (-1.304 \times \ln(Na_2O/SiO_2)_{adj}) + (0.054 \times \ln(K_2O/SiO_2)_{adj}) + (-0.330 \times \ln(P_2O_5/SiO_2)_{adj}) + 1.588$; (2) $DF2_{(Arc\text{-}Rift\text{-}Col)m1} = (1.196 \times \ln(TiO_2/SiO_2)_{adj}) + (1.604 \times \ln(Al_2O_3/SiO_2)_{adj}) + (0.303 \times \ln(Fe_2O_3{}^t/SiO_2)_{adj}) + (0.436 \times \ln(MnO/SiO_2)_{adj}) + (0.838 \times \ln(MgO/SiO_2)_{adj}) + (-0.407 \times \ln(CaO/SiO_2)_{adj}) + (1.021 \times \ln(Na_2O/SiO_2)_{adj}) + (-1.706 \times \ln(K_2O/SiO_2)_{adj}) + (-0.126 \times \ln(P_2O_5/SiO_2)_{adj}) - 1.068$; The subscript m2 in DF1 and DF2 represents the low-silica diagram based on $\log_e$-ratios of major elements. The discriminant function equations are: (1) $DF1_{(Arc\text{-}Rift\text{-}Col)m2} = (0.608 \times \ln(TiO_2/SiO_2)_{adj}) + (-1.854 \times \ln(Al_2O_3/SiO_2)_{adj}) + (0.299 \times \ln(Fe_2O_3{}^t/SiO_2)_{adj}) + (-0.550 \times \ln(MnO/SiO_2)_{adj}) + (0.120 \times \ln(MgO/SiO_2)_{adj}) + (0.194 \times \ln(CaO/SiO_2)_{adj}) + (-1.510 \times \ln(Na_2O/SiO_2)_{adj}) + (1.941 \times \ln(K_2O/SiO_2)_{adj}) + (0.003 \times \ln(P_2O_5/SiO_2)_{adj}) - 0.294$; (2) $DF2_{(Arc\text{-}Rift\text{-}Col)m2} = (-0.554 \times \ln(TiO_2/SiO_2)_{adj}) + (-0.995 \times \ln(Al_2O_3/SiO_2)_{adj}) + (1.765 \times \ln(Fe_2O_3{}^t/SiO_2)_{adj}) + (-1.391 \times \ln(MnO/SiO_2)_{adj}) + (-1.034 \times \ln(MgO/SiO_2)_{adj}) + (0.225 \times \ln(CaO/SiO_2)_{adj}) + (0.713 \times \ln(Na_2O/SiO_2)_{adj}) + (0.330 \times \ln(K_2O/SiO_2)_{adj}) + (0.637 \times \ln(P_2O_5/SiO_2)_{adj}) - 3.631$

probability that clastic sediments of the K_1ml_2 were derived from the collision system, and however, there were possibilities that they may comprise sediments derived from the continental rift system.

Conclusions

Sedimentary rocks collected from the lower Cretaceous Muling Formation (K_1ml) in the Laoheishan basin, northeast China are investigated the petrography, mineralogy and geochemistry to reveal the weathering intensity, provenance and tectonic setting.

Sandstones from the K_1ml_2 have high quartz, medium feldspar and low lithic fragments contents. Lithic fragments are predominantly volcanic clasts. Much gravel has been found from the basement in K_1ml_1 conglomerates. Petrological observation reveals that the sandstones are derived from the surrounding basement and recycled orogeny sources.

Petrography and geochemistry (Al_2O_3/TiO_2, Co/Th, La/Sc, La/Th, Hf) results reveal that the source rocks are mainly felsic and intermediate igneous rocks, probably felsic volcanic rock and andesite. The strong genetic relationship with the igneous rocks from the northwest and northeast indicate the sediments have been derived from this area. The chemical weathering index (CIA) and index of chemical variability (ICV) suggest an intensive weathering in the source region of the sediments.

The multidimensional tectonic discrimination diagrams indicate that the source rocks of K_1ml are predominantly derived from the collision system. However, they may also comprise sediments derived from the continental rift system. These results are consistent with the geology of the study area.

Acknowledgments Authors are grateful to the Editor-in-Chief Lutz Nasdala and Associate Editor M.A.T.M. Broekmans for editorial handling, and to J.S. Armstrong-Altrin and an anonymous reviewer for their constructive and thoughtful comments. The authors thank the support of Opening Foundation of Key Laboratory for Oil Shale and Paragenetic Energy Minerals, Jilin Province. This study was financially supported by the China Geological Survey (1211302108025-5-1) and Graduate Innovation Fund of Jilin University (2016102). Yu Song also thanks the National Construction of High-quality University Projects of Graduates from China Scholarship Council (CSC) (No.201506170120) for an 8-months' scholarship.

References

Armstrong-Altrin JS (2015) Evaluation of two multi-dimensional discrimination diagrams from beach and deep sea sediments from the Gulf of Mexico and their application to Precambrian clastic sedimentary rocks. Int Geol Rev 57(11–12):1446–1461

Armstrong-Altrin JS, Nagarajan R, Lee YI, Kasper-Zubillaga JJ, Cordoba-Saldana LP (2014) Geochemistry of sands along the San Nicolas and San Carlos beaches, Gulf of California, Mexico: implications for provenance and tectonic setting. Turk J Earth Sci 23: 533–558

Armstrong-Altrin JS, Machain-Castillo ML, Rosales-Hoz L, Carranza-Edwards A, Sanchez-Cabeza JA, Ruiz-Fernandez AC (2015a) Provenance and depositional history of continental slope sediments in the Southwestern Gulf of Mexico unraveled by geochemistry analysis. Cont Shelf Res 95:15–26

Armstrong-Altrin JS, Nagarajan R, Balaram V, Natalhy-Pineda O (2015b) Petrography and geochemistry of sands from the Chachalacas and Veracruz beach areas, western Gulf of Mexico, Mexico: Constraints on provenance and tectonic setting. J S Am Earth Sci 64:199–216

Asiedu DK, Suzuki S, Shibata T (2000) Provenance of sandstones from the Lower Cretaceous Sasayama Group, Inner Zone of Southwest Japan. Sediment Geol 131:9–24

Basu A, Young SW, Suttner LJ, James WC, Mack GH (1975) Re-evaluation of the use of undulatory extinction and crystallinity in detrital quartz for provenance interpretation. J Sediment Petrol 45: 873–882

Bhatia MR (1983) Plate tectonics and geochemical composition of sandstones. J Geol 91:611–627

Bhatia MR, Crook KAW (1986) Trace-element characteristics of graywackes and tectonic setting discrimination of sedimentary basins. Contrib Mineral Petrol 92:181–193

Brindley GW, Brown G (1980) Crystal structures of clay minerals and their X-ray identification. Mineralogical Society Monograph 5, London

Camuti KS, McGuire PT (1999) Preparation of polished thin sections from poorly consolidated regolith and sediment materials. Sediment Geol 128:171–178

Cheng RY, Wu FY, Ge WC, Sun DY, Liu XM, Yang JH (2006) Emplacement age of the Raohe Complex in eastern Heilongjiang province and the tectonic evolution of the eastern part of northeastern China. Acta Petrol Sin 22(2):353–376

Condie KC, Phillip DN, Conway CM (1992) Geochemical and detrital mode evidence for two sources of Early Proterozoic sedimentary rocks from Tonto Basin Supergroup, Central Arizona. Sediment Geol 77:51–76

Cox R, Lowe DR, Cullers RL (1995) The influence of sediment recycling and basement composition on evolution of mudrock chemistry in the southwestern United States. Geochim Cosmochim Acta 59: 2919–2940

Cullers RL, Podkovyrov VN (2000) Geochemistry of the Mesoproterozoic Lakhanda shales in southeastern Yakutia. Russia: implications for mineralogical and provenance control, and recycling. Precambrian Res 104:77–93

Cullers RL, Barrett TR, Carlson CR, Robinson B (1987) Rare earth element and mineralogical changes in Holocene soil and stream sediment: a case study in the Wet Mountains, Colorado, USA. Chem Geol 63:275–297

Dickinson WR (1970) Interpreting detrital modes of graywacke and arkose. J Sediment Petrol 40:695–707

Dickinson WR (1985) Interpreting provenance relations from detrital modes of sandstones. In: Zuffa GG (ed) Provenance of arenites. Nato ASI Series C: Math Phys Sci, vol. 48. Springer Netherlands, p 333–361

Dryden AL (1931) Accuracy in percentage representation of heavy mineral frequencies. Proc Natl Acad Sci U S A 17:233–238

Fedo CM, Nesbtit HW (1995) Unravelling the effects of potassium metasomatism in sedimentary rocks and paleosols, with implications for paleoweathering conditions and provenance. Geology 23:921–924

Floyd PA, Leveridge BE (1987) Tectonic environment of the Devonian Gramscatho Basin South Cornwall: framework mode and geochemical evidence from turbiditic sandstones. J Geol Soc Lond 144:531–542

Hanson AD, Ritts BD, Zinniker D, Moldowan JM, Biffi U (2001) Upper Oligocene lacustrine source rocks and petroleum systems of the Northern Qaidam basin, Northwest China. AAPG Bull 85:601–620

Hayashi KI, Fujisawa H, Holland HD, Ohmoto H (1997) Geochemistry of ~1.9 Ga sedimentary rocks from northeastern Labrador, Canada. Geochim Cosmochim Acta 61:4115–4137

Holail HM, Moghazi AKM (1998) Provenance, tectonic setting and geochemistry of greywackes and siltstones of the Late Precambrian Hammamat Group, Egypt. Sediment Geol 116:227–250

Hossain HMZ, Roser BP, Kimura JI (2010) Petrography and whole-rock geochemistry of the Tertiary Sylhet succession, Northeastern Bengal Basin, Bangladesh: provenance and source area weathering. Sediment Geol 228:171–183

Howarth RJ (1998) Improved estimators of uncertainty in proportions, point-counting, and pass-fail test results. Am J Sci 298:594–607

Howarth RJ, French WJ (1998) A statistical study of aggregate testing data with respect to engineering judgement. In: Latham, JP (editor): Advances in aggregates and armourstone evaluation. Geol Soc Eng Geol Sp 13:169–183

Ingersoll RV, Fullard TF, Ford RL, Grimm JP, Pickle JD, Sares SW (1984) The effect of grain size on detrital modes: a test of the Gazzi-Dickinson point-counting method. J Sediment Petrol 54: 103–116

Liu ZH, Mei M, Gao JY, Wu XM, Huang CY, Lin DC, Sun LN (2014) Structural features, formation mechanism of Hulin basin and deformation time of northeastern segment of Dunhua-Mishan fault zone in northeast China. J Jilin Univ (Earth Sci Ed) 44(2):480–489

Luo MS, Lu LQ, Jia J, Wang SD, Xu YD, He WH (2014) Evolution of sedimentary basins in China during Mesozoic. Earth Sci: J China U Geosci 39(8):954–976

Lv DW, Li ZX, Liu HY, Li Y, Feng TT, Wang DD, Wang PL, Li SY (2015) The characteristics of coal and oil shale in the coastal sea areas of Huangxian coalfield, eastern China. Oil Shale 32(3):204–217

Madhavaraju J, Lee YI (2010) Influence of Deccan Volcanism in the sedimentary rocks of Late Maastrichtian-Danian age of Cauvery Basin, Southeastern India: constraints from Geochemistry. Curr Sci India 98:528–537

McCann T (1998) Sandstone composition and provenance of the Rotliegend of the NE German Basin. Sediment Geol 116:177–198

McLennan SM (1989) Rare earth elements in sedimentary rocks: influence of provenance and sedimentary processes. Rev Mineral Geochem 21:169–200

McLennan SM, Hemming SR, Taylor SR, Eriksson KA (1995) Early Proterozoic crustal evolution: geochemical and Nd-Pb isotopic evidence from metasedimentary rocks, southwestern North America. Geochim Cosmochim Acta 59:1153–1177

Migani F, Borghesi F, Dinelli E (2015) Geochemical characterization of surface sediments from the northern Adriatic wetlands around the Po river delta. Part I: Bulk composition and relation to local background. J Geochem Explor 156:72–88

Moore DM, Reynolds RC (1997) X-ray diffraction and the identification and analysis of clay minerals. Oxford University Press, New York

Nagarajan R, Armstrong-Altrin JS, Kessler FL, Hidalgo-Moral EL, Dodge-Wan D, Taib NI (2015) Provenance and tectonic setting of Miocene siliciclastic sediments, Sibuti formation, northwestern Borneo. Arab J Geosci 8:8549–8565

Nesbitt HW, Young GM (1982) Early Proterozoic climates and plate motions inferred from major element chemistry of lutites. Nature 299:715–717

Odoma AN, Obaje NG, Omada JI, Idakwo SO, Erbacher J (2015) Mineralogical, chemical composition and distribution of rare earth elements in clay-rich sediments from southeastern Nigeria. J Afr Earth Sci 102:50–60

Rahman MJJ, Sayem ASM, McCann T (2014) Geochemistry and provenance of the Miocene sandstones of the Surma Group from the Sitapahar anticline, Southeastern Bengal Basin, Bangladesh. J Geol Soc India 83:447–456

Roser BP, Korsch RJ (1986) Determination of tectonic setting of sandstone-mudstone suites using SiO_2 content and K_2O/Na_2O ratio. J Geol 94:635–650

Schultz LG (1964) Quantitative interpretation of mineralogical composition from X-ray and chemical data for the Pierre shale. Geological Survey Professional Paper No. 391-C

Shi GR (2006) Marine Permian in east and NE Asia: an overview of biostratigraphy, palaeobiogeography and palaeogeographical implications. J Asian Earth Sci 26:175–206

Sun XM, Wang SQ, Wang YD, Du JY, Xu QW (2010) The structural feature and evolutionary series in the northern segment of Tancheng-Lujiang fault zone. Acta Petrol Sin 26(1):165–176

Taylor SR, McLennan SM (1985) The continental crust: its composition and evolution. Blackwell Scientific Publications, Oxford

Tucker ME (2009) Sedimentary petrology: an introduction to the origin of sedimentary rocks. John Wiley & Sons, Malden

Verma SP, Armstrong-Altrin JS (2013) New multi-dimensional diagrams for tectonic discrimination of siliciclastic sediments and their application to Precambrian basins. Chem Geol 355:117–133

Verma SP, Armstrong-Altrin JS (2016) Geochemical discrimination of siliciclastic sediments from active and passive margin settings. Sediment Geol 332:1–12

Wronkiewicz DJ, Condie KC (1987) Geochemistry of Archean shales from the Witwatersrand Supergroup, South Africa: source-area weathering and provenance. Geochim Cosmochim Acta 51:2401–2416

Wu FY, Zhao GC, Sun DY, Wilde SA, Yang JH (2007) The Hulan group: Its role in the evolution of the Central Asian Orogenic Belt of NE China. J Asian Earth Sci 30:542–556

Xu WX (2009) Geological characters, metallogenic regularity and model of the gold (copper) ore fields in Jinchang, Heilongjiang Province. China University of Geosciences (Beijing), Dissertation

Xu WL, Wang F, Meng E, Gao FH, Pei FP, Yu JJ, Tang J (2012) Paleozoic-early Mesozoic tectonic evolution in the eastern Heilongjiang province, NE China: evidence from igneous rock association and U-Pb geochronology of detrital zircons. J Jilin Univ (Earth Sci Ed) 42(5):1378–1389

Xu WL, Pei FP, Wang F, Meng E, Ji WQ, Yang DB, Wang W (2013a) Spatial–temporal relationships of Mesozoic volcanic rocks in NE China: constraints on tectonic overprinting and transformations between multiple tectonic regimes. J Asian Earth Sci 74:167–193

Xu ZJ, Cheng RH, Wang LL, Zhang L, Shen YJ, Yu ZF (2013b) Mineralogical and element geochemical characteristics of the late Triassic-Middle Jurassic sedimentary rocks in southwestern Fujian province: constraints on changes of basin tectonic settings. Acta Petrol Sin 29(8):2913–2924

Zaid SM (2013) Provenance, diagenesis, tectonic setting and reservoir quality of the sandstones of the Kareem Formation, Gulf of Suez, Egypt. J Afr Earth Sci 85:31–52

Zhang N, Lin CM, Zhou J, Chen SY, Liu YR, Dong GY (2012) REE characteristics of the 1st member of Eocene Dainan formation in Gaoyou Depression of North Jiangsu Basin, and its significance in provenance instruction. Geol Rev 58:369–378

Zhang N, Lin CM, Zhang X (2014) Petrographic and geochemical characteristics of the Paleogene sedimentary rocks from the North Jiangsu Basin, Eastern China: implication for provenance and tectonic setting. Mineral Petrol 108:571–588

Zhao YS (2013) Porphyry gold system of the Jinchang camp in the Yanbian-Dongning Metallogenic Belt, NE China. China University of Geosciences (Beijing), Dissertation

Zhao YD, Chi XG, Che JY, Liu JF, Zhao Z (2009) Geochemical characteristics and tectonic setting of late Triassic granites in Yanbian-Dongning area. J Jilin Univ (Earth Sci Ed) 39(3):425–434

Zhou JB, Zhang XZ, Ma ZH, Liu L, Jin W, Zhang MS, Wang CW, Chi XG (2009) Tectonic framework and basin evolution in northeast China. Oil Gas Geol 30(5):530–538

Zhou L, Friis H, Poulsen MLK (2015) Geochemical evaluation of the late Paleocene and early Eocene shales in Siri Canyon, Danish-Norwegian basin. Mar Pet Geol 61:111–122